Scripta Materialia 124 (2016) 67–70

Contents lists available at ScienceDirect

Scripta Materialia

journal homepage: www.elsevier.com/locate/scriptamat

Regular Article

Superlattice effect for enhanced fracture toughness of hard coatings

R. Hahn [a,b,*], M. Bartosik [a,b], R. Soler [c], C. Kirchlechner [c,d], G. Dehm [c], P.H. Mayrhofer [a,b]

[a] Institute of Materials Science and Technology, TU Wien, A-1060 Vienna, Austria
[b] Christian Doppler Laboratory for Application Oriented Coating Development at the Institute of Materials Science and Technology, TU Wien, A-1060 Vienna, Austria
[c] Max-Planck-Institut für Eisenforschung, Max-Planck-Straße 1, D-40237 Düsseldorf, Germany
[d] Department Material Physics, University of Leoben, A-8700 Leoben, Austria

ARTICLE INFO

Article history:
Received 9 May 2016
Received in revised form 23 June 2016
Accepted 24 June 2016
Available online 6 July 2016

Keywords:
Fracture toughness
Superlattice toughness
Nanolayer
Hard coatings
Micromechanical testing

ABSTRACT

Coherently grown nanolayered TiN/CrN thin films exhibit a superlattice effect in fracture toughness, similar to the reported effect in indentation hardness. We found –by employing *in-situ* micromechanical cantilever bending tests on free-standing TiN/CrN superlattice films– that the fracture toughness increases with decreasing bilayer period (Λ), reaching a maximum at $\Lambda \sim 6$ nm. For ultrathin layers ($\Lambda \sim 2$ nm), the fracture toughness drops to the lowest value due to intermixing and loss of superlattice structure. Both, fracture toughness and hardness peak for similar bilayer periods of TiN/CrN superlattices.

Hard coatings are used to protect engineering components, e.g. cutting tools, from severe external loads and harsh environments [1]. Thereby, the coatings should ideally be strong and tough. Multilayer coatings composed of two coherently stacked, alternating materials with a periodicity length in the nanometer range, referred to as superlattice films, have been reported to possess exceptional high hardness values exceeding that of their single layered constituents by some hundred percent. In the 1980s, Helmersson et al. [2] reported on a hardness enhancement of up to ~250% compared to single-layered materials for the single-crystalline coherent TiN/VN superlattice (SL) structure grown by physical vapor deposition on single crystalline MgO (100) substrates. Thereby, the peak hardness was found for a periodicity length of ~5 nm. Later, an hardness enhancement was observed for a row of other SL film systems grown on MgO (100), but also on (native oxide) of Si (100) and polycrystalline steel substrates [3].

Besides high hardness values, a sufficiently high fracture toughness is needed to ensure the integrity of bulk and coated engineering components. Unfortunately, these material properties are commonly mutually influential (especially for materials showing plastic behavior), as a high strength often implies a low fracture toughness and vice versa [4]. In the last decades various strategies have successfully shown how to break down this relationship, spanning from grain refinement toughening –based on the classical Hall-Petch relation used in a variety of steels [5,6]– to recently found nanoscaled twinning mechanisms being operative in high-entropy alloys –enabling exceptional high fracture-resistance even at cryogenic temperatures [7]– and several other mechanisms presented in Ref. [4]. Strategies for enhancing the (fracture) toughness of ceramic coatings (see review by Zhang et al. [8]) include: incorporating a ductile phase; toughening through a nanocrystalline microstructure, composition, or structure grading; multilayer structuring; phase transformation toughening; or apparent toughening by implementation of compressive stresses, most of them being already effectively applied in industrial products. However, the exceptional effect of a superlattice structure on the fracture toughness has yet not been reported.

Here, we study the influence of the superlattice structure on the fracture toughness. Therefore, we have conducted micromechanical experiments on freestanding superlattice coatings with different bilayer periods (Λ). The isomorphous face-centered cubic (B1) TiN/CrN superlattice grown on Si (100) substrates served as a model system. The constituents TiN and CrN represent one of the most widely used nitrogen-based hard coating materials and their shear moduli (~180 GPa [9] and ~135 GPa [10], respectively) are significantly different, which promotes the superlattice effect [11].

TiN/CrN multilayer films with equal thick layers –bilayer periods ranging from ~2 to 200 nm, and total film thicknesses of ~2 μm– were synthesized by dc unbalanced reactive magnetron sputtering. All films were grown on Si (100) substrates ($7 \times 20 \times 0.38$ mm^3) in an AJA International Orion 5 magnetron sputtering system equipped with one two-inch Cr and one three-inch Ti target (both from Plansee Composite Materials GmbH, 99.6 at.% purity). Prior to the deposition, the substrates

* Corresponding author at: Institute of Materials Science and Technology, TU Wien, A-1060 Vienna, Austria.
E-mail address: rainer.hahn@tuwien.ac.at (R. Hahn).

http://dx.doi.org/10.1016/j.scriptamat.2016.06.030

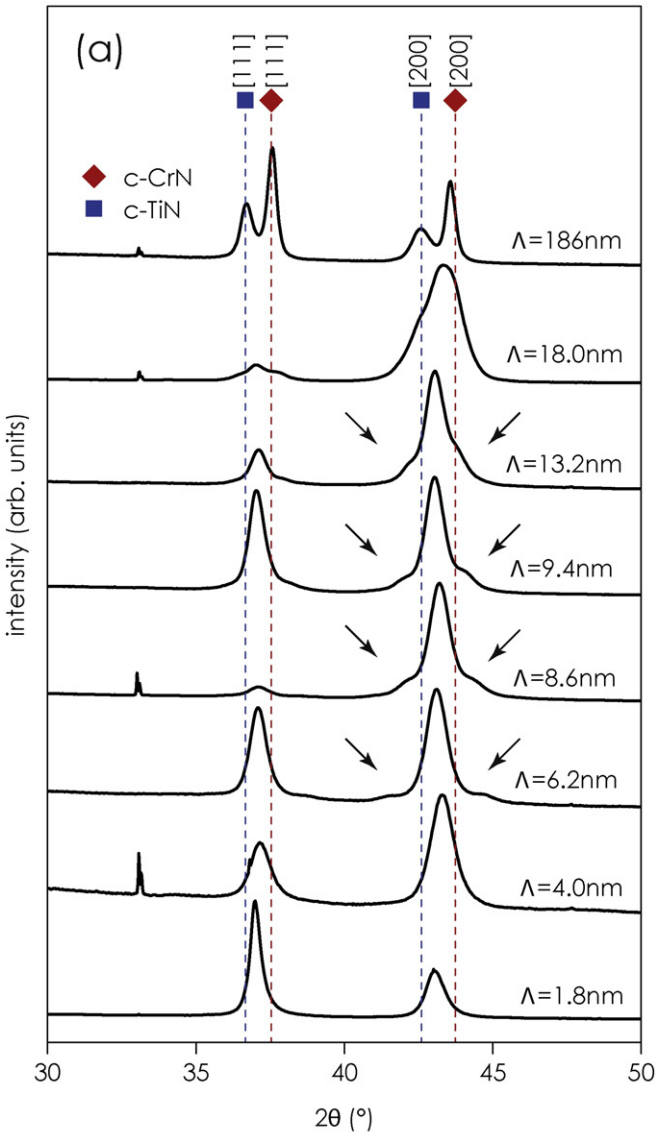

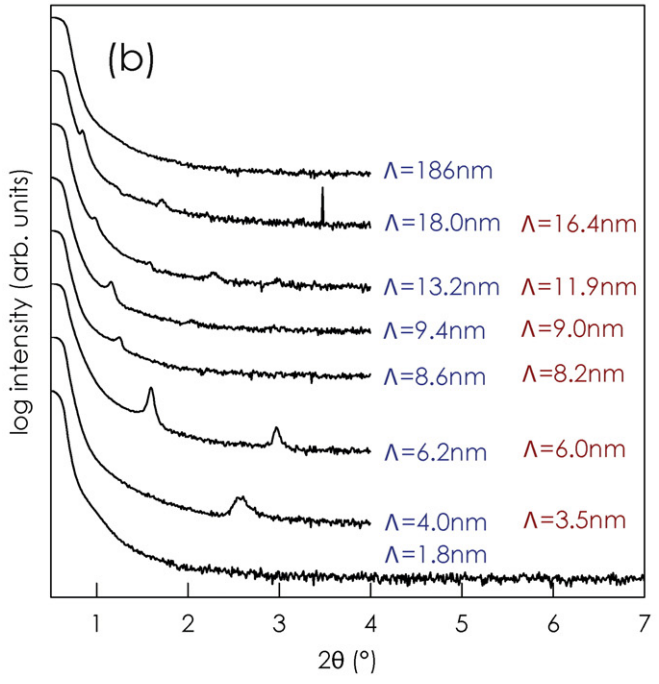

were ultrasonically cleaned in ethanol and acetone, for 5 min each. Subsequently, the substrates were mounted inside the deposition chamber (evacuated to a base pressure below 10^{-4} Pa), thermally cleaned at 500 °C for 20 min, and Ar-plasma etched (Ar pressure = 6 Pa) at the same temperature for 10 min. The deposition was carried out at 500 °C in an Ar/N_2 gas mixture with a flow ratio of 1/1 and a total pressure of 0.4 Pa. Both targets were dc powered using a target power density of 6.8 W/cm^2 for Ti and 7.6 W/cm^2 for Cr. To ensure a dense film morphology, a constant negative bias potential of −60 V was applied to the substrates. The alternating and equally thick TiN and CrN layers were deposited by using a computer controlled shutter system mounted in front of the Ti and Cr targets. Films with the following nominal bilayer periods (obtained by dividing the total film thickness with the number of TiN/CrN pairs) were synthesized: 1.8, 4.0, 6.2, 8.6, 9.4, 13.2, 18.0, and 186 nm. To highlight the superlattice effect itself, we intentionally used only a moderate bias potential of −60 V during the deposition of our polycrystalline TiN/CrN thin films, although Barshilia et al. [12], for instance, reported even higher peak hardnesses for TiN/CrN superlattice films when prepared with high bias potentials of −150 V.

X-ray diffraction (XRD) patterns from all coatings were collected in symmetric Bragg-Brentano configuration using Cu-K_α radiation and are presented in Fig. 1(a). The XRD patterns show that the films grew in the face-centered cubic crystal structure. Cumulative diffraction peaks with peak positions laying in between TiN and CrN peaks (instead of two clearly differentiate peaks) reveal the presence of a superlattice structure with strained layers. Furthermore, positive and negative satellite peaks reflecting the SL structure (marked exemplarily with arrows in Fig. 1(a) in the vicinity of the 200 Bragg peak) emerge for the Λ = 6.2 nm multilayer film and become more apparent with increasing bilayer period. In the case of the multilayer film with the thickest bilayer period (Λ = 186 nm), two clearly separated Bragg peaks matching TiN and CrN lattice constants are observed, suggesting a largely independent growth of TiN and CrN layers with incoherent or semi-coherent interfaces, as expected for large bilayer periods. The native oxides on the Si (100) substrates lead to the formation of a polycrystalline structure within all our thin films.

In order to confirm the estimated nominal bilayer periods we conducted X-ray reflectivity (XRR) measurements, Fig. 1(b), and used a modified Braggs-law approach to calculate Λ:

$$sin^2(\theta) = \left(\frac{m * \lambda}{2 * \Lambda}\right)^2 + 2 * \delta, \tag{1}$$

where m denotes the order of the reflection, λ the wavelength of radiation (here Cu-K_α) and δ the real part of the average refractive index (in our case $\delta \sim 1.6 * 10^{-5}$) [13]. The XRR obtained bilayer periods excellently fit to the nominal bilayer periods, see the listed values in Fig. 1b. The XRR patterns show no signs for a superlattice structure for our thin films with the largest and smallest nominal bilayer periods (Λ = 186 and 1.8 nm), hence, no XRR obtained bilayer periods could be calculated for these. This suggests that for our thin film with the smallest nominal bilayer period of 1.8 nm, the intermixing interface regions between TiN and CrN layers are too dominant to allow for the development of a superlattice structure. These results are further supported

Fig. 1. XRD (a) and XRR (b) scans of TiN/CrN superlattice films with different bilayer periods Λ The arrows in (a) exemplarily mark satellite peaks in the vicinity of the 200 Bragg peak reflecting the SL structure. The bilayer periods quoted in the left column (blue) in (b) were calculated by dividing the total film thickness through the number of TiN/CrN pairs (obtained from the computer controlled deposition system), those in the right column (red) were calculated from the 2θ peak-positions. The coatings with the thickness-obtained Λ of 1.8 nm and 186 nm show no signs of a superlattice structure.

by transmission electron microscopy (TEM) cross section images, Figs. 2(a) and (b). In contrast to our thin film with a nominal Λ of 13.2 nm (exhibiting a pronounced superlattice structure) no layered structure can be observed for the sample with a nominal Λ of 1.8 nm, explaining the missing XRR peak. The TEM samples were prepared by conventional grinding of a film-substrate lamella down to a thickness of ~10 μm using a diamond abrasive. A GATAN Precise Ion Polishing System was used to further thin the sample down till electron transparency. The TEM-images were recorded using a FEI TECNAI F20 operating with an acceleration voltage of 200 kV.

To determine the fracture toughness of all TiN/CrN thin films, micromechanical single cantilever bending tests were performed on free-standing films. This approach allows to effectively eliminate potential sources of errors, like the influence of the substrate material and residual film stresses on the fracture toughness [14]. The Si substrates were locally dissolved by 90 min wet chemical etching in a 30 wt.% potassium hydroxide (KOH) solution heated to 60 °C. As a result, free-standing films (~20 μm broad and a few mm wide) were obtained. Cantilevers with dimensions of ~2 × 2 × 14 μm^3 were fabricated by Ga^+ focused ion beam (FIB) milling perpendicular to the film surface, using a FEI Quanta 200 3D DBFIB work station. A final milling current of 500 pA at an acceleration voltage of 30 kV was employed. The pre-notch was milled using 50 pA. A scanning electron microscope image (30° inclined from top view) of a pre-notched single cantilever specimen after FIB milling is depicted in Fig. 3(a).

The in-situ micromechanical experiments were performed in a JEOL scanning electron microscope (JEOL JSM 6430, JEOL Ltd., Akishima, Japan) equipped with an UNAT SEM-2 nanoindenter (ASMEC GmbH, Radeberg, Germany). A 2 μm spherical diamond tip was used for the experiments. The tests were carried out on a displacement-controlled mode, at a constant displacement rate of 5 nm/s. For each multilayer film system, 10 μ-beams were tested (with an average success rate of ~76%). Representative load-deflection curves for the SL films with Λ = 1.8, 6.2, and 18.0 nm are shown in Fig. 3(b). Note that deviations on loading stiffness arise for different cantilevers due to small variations on actual cross-sections and distances of applied load, *l*. Nonetheless, all

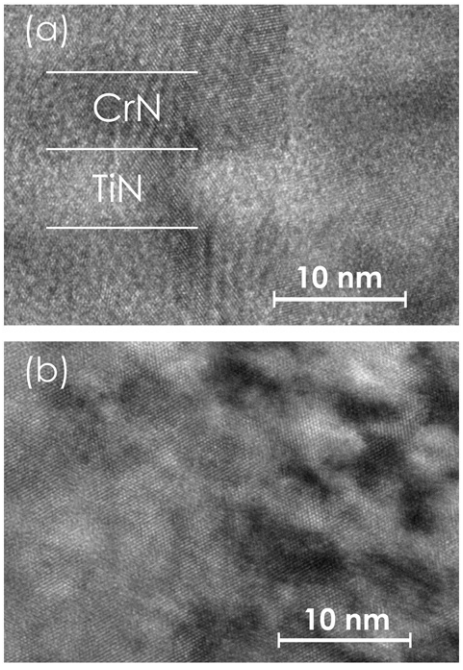

Fig. 2. HR-TEM images of the TiN/CrN superlattice films exhibiting bilayer periods of 13.2 (a) and 1.8 nm (b), respectively. While the nanolayered structure can be clearly seen for the large bilayer period sample (a) the interdiffusion-areas between TiN and CrN and loss of the layer structure becomes evident for the smallest bilayer period samples shown in (b).

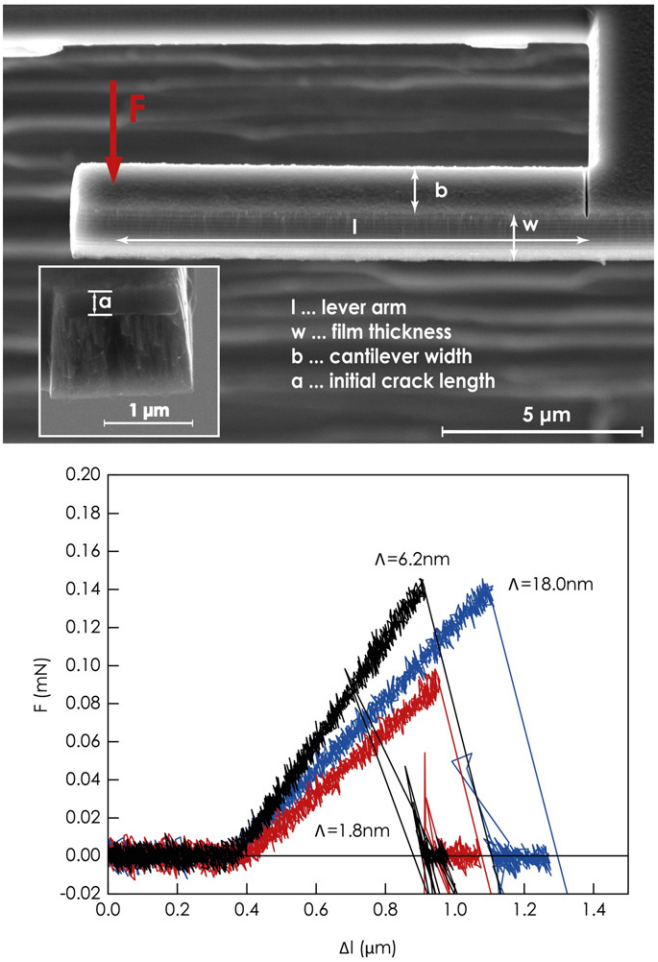

Fig. 3. (a) Scanning electron microscope image (30° inclined from top view) of a pre-notched single cantilever specimen before micromechanical testing. The insert is a post mortem SEM image of the fractured surface showing pre-notch depth *a*. (b) Representative bending stress-deflection curves recorded in the micromechanics single cantilever bending experiments from TiN/CrN superlattice films with bilayer periods of 1.8, 6.2 and 18.0 nm.

SL structures present a perfect linear-elastic brittle fracture behavior without any signs of plasticity in the load-displacement response. Therefore, linear-elastic fracture mechanics was applied to quantify the fracture toughness K_{IC}:

$$K_{IC} = \frac{P_{max} * l}{b * w^{3/2}} * f\left(\frac{a}{w}\right), \tag{2}$$

whereby the geometry factor $f(\frac{a}{w})$ was taken as:

$$f\left(\frac{a}{w}\right) = 1.46 + 24.36 * \left(\frac{a}{w}\right) - 47.21 * \left(\frac{a}{w}\right)^2 + 75.18 * \left(\frac{a}{w}\right)^3, \tag{3}$$

according to Matoy et al. [15]. P_{max} denotes the maximum force, *l* the lever arm, *b* the width of the cantilever, and *w* the film thickness (see Fig. 3(a)). The initial crack length, *a*, was determined from SEM micrographs of the post mortem fracture surface, as shown in an example in the insert of Fig. 3(a). The relatively flat fracture surface together with the absence of dimples or any other sign of significant plastic deformation, confirm the brittle fracture response of our thin films.

The derived fracture toughness (K_{IC}) vs. the bilayer period for all superlattices studied – as well as those of the thin films with a nominal Λ of ~186 and 1.8 nm– is presented in Fig. 4 showing a pronounced bilayer-period-dependent behavior. For large bilayer periods ($\Lambda \geq$ 13 nm), K_{IC} remains relatively constant, at ~1.65 ± 0.1 MPa$\sqrt{m}$. For smaller

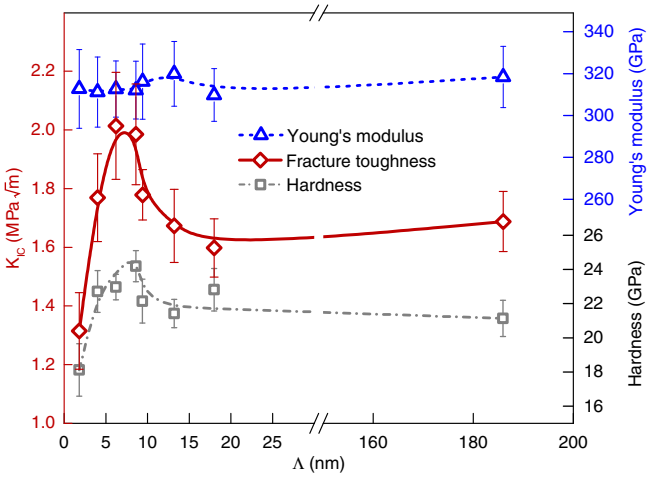

Fig. 4. Fracture toughness K_{IC}, indentation hardness H and moduli E of our TiN/CrN superlattice thin films as a function of their bilayer period Λ The individual data points are connected to guide the eye.

bilayer periods, K_{IC} significantly raises, reaching a maximum value of ~2.01 ± 0.18 MPa√m at Λ ~ 6.2 nm. Further decreasing Λ drops dramatically K_{IC} to a minimum value of ~1.31 ± 0.13 MPa√m at Λ ~ 1.8 nm. Interestingly, a very similar dependency is observed for the hardness measurements, with H vs. Λ exhibiting a hardness peak with 24.2 ± 0.9 GPa at Λ ~ 8.6 nm. The agreement between K_{IC} vs. Λ and H vs. Λ suggests that similar bilayer-period-dependent mechanisms could be responsible for both, the indentation hardness and the fracture toughness enhancement. The relatively constant indentation modulus as a function of the bilayer period, E vs. Λ, further proofs our K_{IC} vs. Λ curve by the coincidence with the H/E empirical criteria, often used to qualitatively rate materials for their toughness [16,17]. This simplified criterion predicts for brittle materials with similar E values, that a higher hardness would result in a higher energy absorbed until fracture.

The hardness enhancement due to the superlattice effect, described by the model after Chu and Barnett [18], is based on two mechanisms being operative during plastic deformation of a superlattice system. For small bilayer periods, the stresses required for dislocations to glide across layers with different shear moduli increase with increasing bilayer periods. The second mechanism describes the stress required to move preexisting dislocations within the layers, as well as the stress required to activate dislocation sources. The latter two required stresses, τ, decrease with increasing bilayer period, following a Hall-Petch-like relationship:

$$\tau \propto \Lambda^{-m}. \tag{4}$$

According to Chu and Barnett [18] the hardness enhancement in superlattices is, therefore, a plasticity driven phenomenon, and as such, is governed by dislocation mobility. In contrast, the herein presented fracture experiments show an absence of plastic deformation, hence, behave in a linear-elastic brittle manner. In this case the failure of the material is controlled by the average defect density and average maximum defect size. Thereby, rather than a bilayer-period-dependent dislocation-based mechanism, there must be an underlying bilayer-period-dependent property governing both SL effects. Some of these bilayer-period-dependent properties might be: coherency strains; misfit dislocation arrays at the interface; spatially oscillating elastic moduli influencing crack growth; average grain size and other defects confined into individual layers.

It is yet to be discovered which intrinsic SL property is responsible for the fracture toughness enhancement. But based on our results, a power-law relationship similar as for τ will hold between the fracture toughness and the bilayer period:

$$K_{IC} \propto \Lambda^{-m}, \tag{5}$$

with the exponent m depending on the type and interface constitution of the superlattice structure. The exponent m equals roughly 0.25 for our superlattice TiN/CrN coatings with $\Lambda \geq 6.2$ nm.

The decline in H as well as K_{IC} when further reducing the bilayer period (below ~6 nm) is also based on the decreasing SL effect, as with smaller bilayer periods the intermixing interface-regions between both layer types become dominant – see Figs. 1(b) and 2(b) and the missing signs for a superlattice structure with a nominal Λ of 1.8 nm.

Based on our results on polycrystalline TiN/CrN SL structures –deposited by unbalanced magnetron sputtering with different bilayer periods on Si (100) substrates– we can conclude, that a significant increase in fracture toughness is observed when SL structures are formed, similar to the well-known SL effect on hardness. However, further investigations into the toughening mechanisms are required in order to better understand this behavior and how it relates to the hardness SL effect. This new superlattice effect represents a significant improvement in mechanical properties of hard thin films, especially when both, hardness and fracture toughness, are simultaneously enhanced as it is the case here.

Acknowledgements

The financial support by the START Program (Y371) of the Austrian Science Fund (FWF) is gratefully acknowledged. SEM, TEM, and XRD investigations were carried out using facilities of the XRC and USTEM centers of TU Wien, Austria. The financial support by the Austrian Federal Ministry of Economy, Family and Youth and the National Foundation for Research, Technology and Development are gratefully acknowledged. The work of RS has been conducted within the project EPPL, co-founded by grants from Austria, Germany, The Netherlands, France, Italy, Portugal and the ENIAC Joint Undertaking.

References

[1] P.H. Mayrhofer, A. Hörling, L. Karlsson, J. Sjölén, T. Larsson, C. Mitterer, L. Hultman, Appl. Phys. Lett. 83 (2003) 2049.
[2] U. Helmersson, S. Todorova, S.A. Barnett, J.-E. Sundgren, L.C. Markert, J.E. Greene, J. Appl. Phys. 62 (1987) 481.
[3] M. Stueber, H. Holleck, H. Leiste, K. Seemann, S. Ulrich, C. Ziebert, J. Alloys Compd. 483 (2009) 321.
[4] R.O. Ritchie, Nat. Mater. 10 (2011) 817.
[5] J.W. Morris, The Influence of Grain Size on the Mechanical Properties of Steel, Lawrence Berkeley National Laboratory, 2001.
[6] M. Calcagnotto, D. Ponge, D. Raabe, Mat. Sci. Eng. A 527 (2010) 7832.
[7] B. Gludovatz, A. Hohenwarter, D. Catoor, E.H. Chang, E.P. George, R.O. Ritchie, Science 345 (2014) 1153.
[8] S. Zhang, D. Sun, Y. Fu, H. Du, Surf. Coat. Technol. 198 (2005) 2.
[9] D. Holec, M. Friák, J. Neugebauer, P.H. Mayrhofer, Phys. Rev. B 85 (2012) 064101.
[10] L. Zhou, D. Holec, P.H. Mayrhofer, J. Appl. Phys. 113 (2013) 043511.
[11] M. Shinn, S.A. Barnett, Appl. Phys. Lett. 64 (1994) 61.
[12] H.C. Barshilia, A. Jain, K.S. Rajam, Vacuum 72 (2004) 241.
[13] P.C. Yashar, W.D. Sproul, Vacuum 55 (1999) 179.
[14] B.N. Jaya, C. Kirchlechner, G. Dehm, J. Mater. Res. 30 (2015) 686.
[15] K. Matoy, H. Schönherr, T. Detzel, T. Schöberl, R. Pippan, C. Motz, G. Dehm, Thin Solid Films 518 (2009) 247.
[16] B.R. Lawn, A.G. Evans, D.B. Marshall, J. Am. Ceram. Soc. 63 (1980) 574.
[17] A.G. Evans, E.A. Charles, J. Am. Ceram. Soc. 59 (1976) 371.
[18] X. Chu, S.A. Barnett, J. Appl. Phys. 77 (1995) 4403.